Efficient photocatalytic fixation of N_2 by KOH-treated g-C_3N_4†

Xiaoman Li,[ab] Xiang Sun,[ab] Ling Zhang, [a] Songmei Sun[a] and Wenzhong Wang *[a]

Development of N_2 photofixation under mild conditions is challenging; one reason for low efficiency is the poor reactivity between water and photocatalysts. Herein, C_3N_4 after KOH etching was used as an efficient photocatalyst, and CH_3OH was first introduced as a proton source. The photocatalyst presented a high ammonia evolution rate of 3.632 mmol g^{-1} h^{-1} and achieved an apparent quantum yield of 21.5% at 420 nm. In addition to the role of reacting with holes to accelerate the production and transfer of electrons, CH_3OH also promoted the solubility of N_2 and provided a proton to the activated N_2. The CH_3OH system should be instructive for a better understanding of proton-enhanced photocatalysis.

Introduction

Nitrogen makes up 78% of the atmosphere, but it is a limiting nutrient for biomass production.[1] The strong (944.84 kJ mol^{-1}), unpolarized triple bond of nitrogen (N_2) is the reason of its weak reactivity.[2] There are great demands for fertilizers in agriculture and ammonia in the industry. Worldwide attention has been paid to artificial nitrogen fixation. The most efficient artificial method of nitrogen fixation is the Haber–Bosch process since 1917.[3] However, the drawback of the Haber–Bosch reaction is its high energy consumption due to high-temperature (400–500 C) and high-pressure (150–250 atm) requirements of the process.[4] Recently, photocatalysis has become an attractive method for nitrogen fixation because it is an environmentally friendly and energy-saving process that occurs at room temperature and atmospheric pressure. During this process, photocatalysts convert solar energy into energetic electrons and holes; then, the carriers can migrate to the reactive sites and catalyze the adsorbed nitrogen as well as water to produce ammonia.

Nitrogen photo fixation was first achieved under UV irradiation on an Fe-doped TiO_2 powder by Schrauzer and Guth in 1977.[5] After this, many groups tried to optimize the photo-catalytic efficiency. Many experimental[6] and theoretical studies[7] have shown that N_2 dissociation is the rate-limiting step. Thus, some researchers explored different kinds of photocatalysts with useful active sites, such as an oxygen vacancy on BiOBr,[8] unsaturated carbon on H_2WO_4,[9] nitrogen vacancy on g-C_3N_4,[10] and nanoscale BiO QDs,[11] which can increase the dissociative adsorption of N_2 and promote the cleavage of the N^N triple bond. In addition to those reported on N_2 dissociation, studies on the process of electron and proton transfer have also been reported. Some studies focussed on the electron transfer in the reduction course. Chen's group[12] confirmed that hot electrons from an iron- and graphene-based catalyst induced by visible light could efficiently facilitate the activation of N_2 and generate ammonia directly. Our previous study[13] found that multi-electron transfer that existed in ultrathin MoS_2 resulted in light-induced trions, which achieved a higher ammonia synthesis rate. For the hydrogenation of N_2, instead of using this conventional energy-inefficient hydrocarbon / H_2 / H reaction, hydrogen atoms could be directly generated via a shortcut, green route using sunlight and a water photo-splitting setup through a proton photo-reduction reaction ($H^+ + e_{CB}$ / H) on a semiconductor material.[14]

However, the studies on the water-derived proton transfer only focused on the change in the pH values in the reaction system as pH could increase the concentration and decrease the energy barrier of the proton reduction. Usually, hydrogen can be generated by aqueous-phase reforming of biomass-derived carbohydrates, including methanol, on platinum/aluminium oxide catalysts. On the other hand, the solubility of N_2 in methanol was 10 times higher than that in water; this increased the reaction rate of nitrogen fixation. Thus, to achieve the goal of increasing the proton crack, we changed the proton source from water to methanol first. CH_3OH not only provided protons, but also reacted with photo-induced holes and increased the concentration of reactive electrons. Further facial modification of the g-C_3N_4 photocatalyst with KOH enhanced the ammonia evolution rate through the exposed active sites and the doping of potassium. The mechanism of nitrogen fixation on C_3N_4–CH_3OH was speculated to be the Mars-van Krevelen (MvK) mechanism. The photocatalyst achieved a high apparent quantum yield of 21.5% at around 420 nm.

[a]State Key Laboratory of High Performance Ceramics and Super ne Microstructures, Shanghai Institute of Ceramics, Chinese Academy of Sciences, 1295 Dingxi Road, Shanghai 200050, P. R. China. E-mail: wzwang@mail.sic.ac.cn

[b]University of Chinese Academy of Sciences, Beijing 100049, P. R. China

Results and discussion

g-C_3N_4 (denoted as CN) was prepared via a common method of urea thermal polymerization.[15] C_3N_4, such as nitrogen vacancy-containing g-C_3N_4 (ref. 10) and microwave-synthesized g-C_3N_4, has been applied in nitrogen photo xation.[16] The nitrogen defect in C_3N_4 improved the activation of nitrogen. Acid or alkaline treatment[17–19] is a simple and effective way for improving the multiple performance of g-C_3N_4. The treatments improved the activity of g-C_3N_4 for the corresponding demands of application performance. In this study, CN was further treated with KOH at different concentrations (named as CNK0.1, CNK0.5, CNK1, and CNK3). The purpose of introducing KOH was not only to strengthen vacancy-induced defect states and carrier transfer efficiency, but also to graft potassium on the surface of catalysts for promoting ammonia desorption.[20] Microstructures of the as-prepared samples were observed by transmission electron microscopy (TEM). Contrary to the research where KOH is mixed with the precursor of C_3N_4 before thermal polymerization,[21] the directly infiltrated C_3N_4 in the KOH solution in this study brings about macroscopic holes on the surface. As presented in Fig. 1, the pristine CN particles showed a smooth surface (Fig. 1a), but the samples with C_3N_4 etched by KOH (CNK) presented pores on the entire surface with a relatively uniform pore size (Fig. 1b). After treatment with the KOH solution, CN with larger layer surfaces (Fig. S1†) was fragmented to CNK with a small surface area (Fig. S2†). The crystallographic structure and phase purity of the as-prepared samples were examined by X-ray diffraction (XRD) analysis. The (100) peaks of CNKs became weaker and broader than those of the CN sample probably due to the decrease in the order degree of the in-plane structural packing. Moreover, a red-shift of the (002) peaks in CNKs following the increased concentration of KOH was observed. The decrease in the distance between the layers could be attributed to the incorporation of K atoms between the CN layers, and these incorporated K atoms hold the layers tightly.

The compositions and chemical states of CN and CNKs were further researched by X-ray photoelectron spectroscopy (XPS). To examine the influence of the alkali, pristine C_3N_4 was treated with a 1 M KCl solution through the same method as that of KOH etching, labeled as CN–KCl. As shown in Fig. 1d, the spectra of K 2s indicated that potassium existed in CNK, and the content of K increased in direct proportion to the concentration of the KOH solution. However, potassium was lacking in the CN–KCl sample; this indicated that the decoration of K depended on the alkali, and K could not be grafted onto CN in a neutral solution. The high-resolution spectra of C 1s and N 1s are presented in Fig. 1e and f, and both the binding energies of C 1s in the s-triazine rings (N–C–N, 288.1 eV)[22] and the binding energies of N 1s in the s-triazine rings (C–N–C, 398.5 eV)[23] increased in CNKs as compared with those in CN–KCl. The higher binding energies of CNKs indicated that the s-triazine rings of C_3N_4 were broken in the KOH solution, and the C–N]C coordination became more active. However, in particular, the C 1s and N 1s peaks of CNK3 in the s-triazine rings were lower than those of CNK1. The K state in CNK was further explored, and the high-resolution K 2p spectra are shown in Fig. S3.† The peak locations of K $2p_{3/2}$ and K $2p_{1/2}$ of CNK1, CNK0.5, and CNK0.1 are the same as those of the potassium salt (K^+).[24] Interestingly, the K $2p_{3/2}$ and K $2p_{1/2}$ peaks of CNK3 are located at 292.7 eV and 295.3 eV, which are lower than those of the potassium salt; this indicates the existence of a covalent bond between K and C_3N_4. These results suggested that the higher KOH concentration ($3 M) brought greater damage to the s-triazine rings of C_3N_4; thus, K^+ in KOH was adsorbed onto the rings to balance the breakage. KOH at lower concentrations (0.1, 0.5, and 1 M) caused a so crack on C_3N_4, and K^+ bonded C_3N_4 through van der Waals forces. Porous g-C_3N_4 nanosheets were also synthesized *via* direct pyrolysis of thiourea followed by thermal exfoliation, as detailed in previous research.[25] However, potassium also played an important role in the ammonia evolution, and the KOH treatment was necessary.

To further determine the structure of the samples, the measurements of Fourier transform-infrared (FT-IR) (Fig. 1h) spectroscopies were considered. The bands at 811 cm^{-1} of the CNK samples were assigned to the ring breathing of the triazine unit,[26] which slightly shifted towards lower frequencies as compared to those of the pristine CN sample; this suggested that the coordination environment of N]C–N covalent bonds changed. The band at 1687 cm^{-1} could be attributed to the stretching vibration of C]N,[27,28] which disappeared in CNK. It confirmed that the breakage of the C]N bond when C_3N_4 was stirred in the KOH solution and the higher concentration caused more changes in the structure. The band peaks at 3440 cm^{-1} corresponding to the O–H stretching vibrations only existed in the CNK samples;[29] this indicated that the hydroxyl group was also adsorbed on the surface of the broken C_3N_4. Additionally, Raman spectra of CNKs are shown in Fig. 1g, and the results are consistent with those of the FTIR spectra.[30,31] The triazine peak (714 cm^{-1}) in CNKs shifted, and one of the C]N peaks (776 cm^{-1}) in CNKs disappeared; this confirmed the crack on the surface structure and nitrogen vacancies in the CNK. In addition, the BET surface areas calculated from the N_2 adsorption–desorption curves of the unmodified and all the CNK samples were very close to each other, as listed in Table S1.† This indicated that the preparation processes had little influence on the macrostructure of g-C_3N_4.

To assess the validity of using CH_3OH and KOH for improving the photocatalytic efficiency, photocatalytic ammonia evolution of the as-prepared samples was carried out. As exhibited in Fig. 2a, all CNKs showed greatly superior activities than pristine carbon nitride in a 100% CH_3OH solution under AM 1.5 G illumination. The ammonia evolution rate of pristine CN–KCl was 0.913 mmol g^{-1} h^{-1}, which was close to that of the pristine CN sample. The unchanged structure of CN– KCl and the same rate between CN and CN–KCl confirmed that the alkali salt could not affect the bonding of s-triazine in the CN sample, and K^+ would not be grafted on the pristine uncracked CN layers. The ammonia evolution rate of carbon nitride obtained in 1 M KOH was 3.632 mmol g^{-1} h^{-1}, which was 4 and 1.5 times higher than that of pristine CN and CNK0.1, respectively. The improvement of the ammonia generation rate

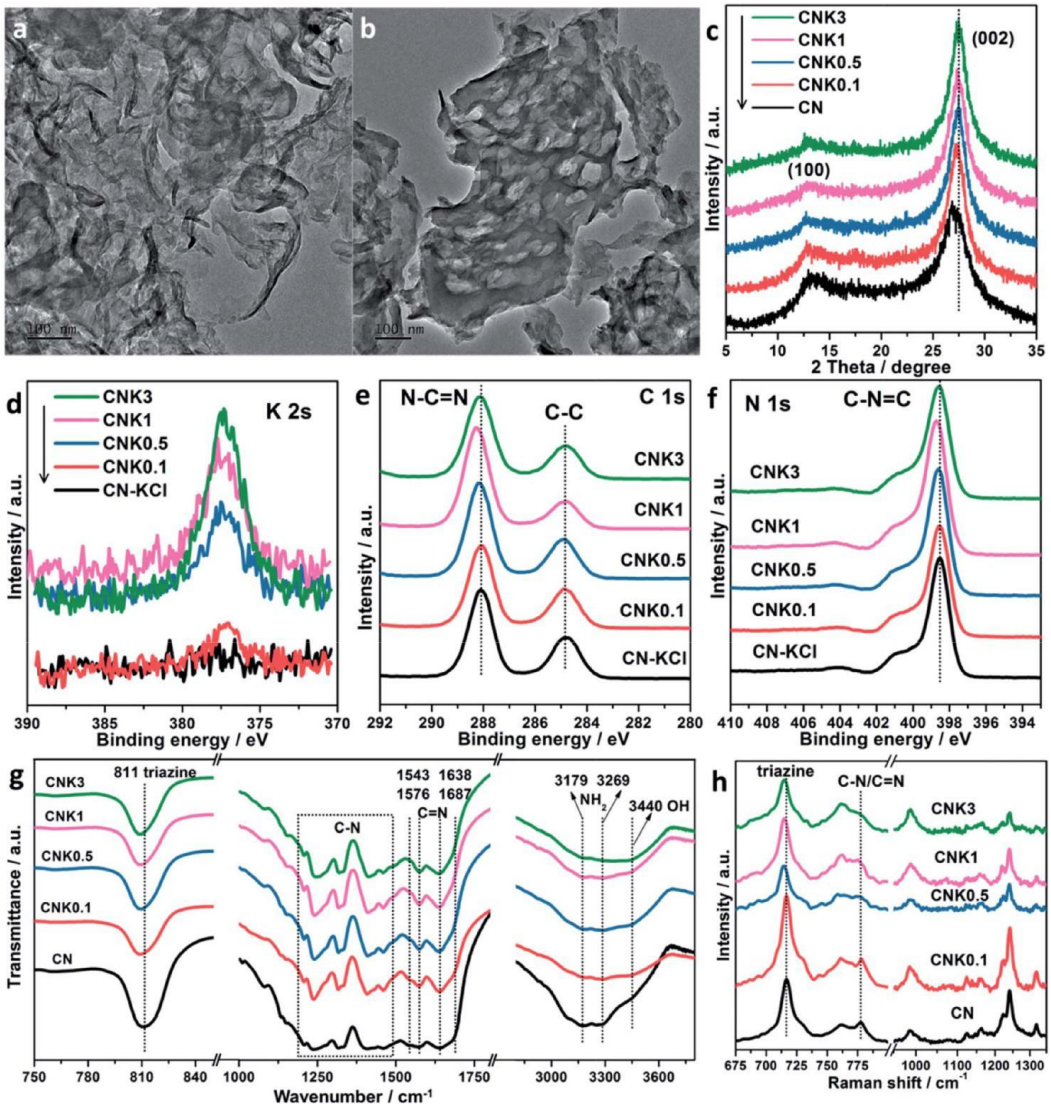

Fig. 1 Characterizations of the g-C_3N_4 and CNK samples. (a) TEM image of CN, (b) TEM image of CNK, the scale bar of (a and b) is 100 nm, (c) XRD patterns, (d–f) XPS spectra, (g) FTIR spectra, and (h) Raman spectra.

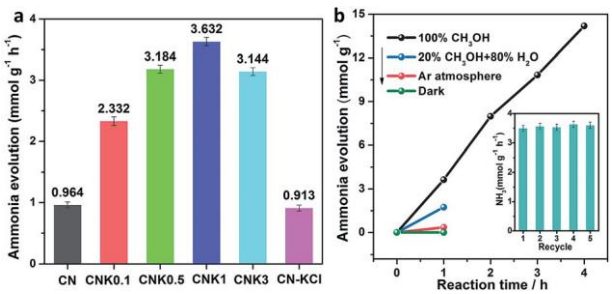

Fig. 2 Nitrogen fixation rate of the prepared samples under AM 1.5 G illumination. (a) Comparison of CN and CNKs and (b) ammonia evolution with time of CNK1; inset shows the cycling experimental performance of CNK1.

after etching of KOH verified the prospect that the more exposed active sites and the grafting of potassium increased the ammonia desorption efficiency. CNK3 presented a lower ammonia generation rate as compared to CNK1. It was speculated that potassium adsorbed on the active sites of CNK3; thus, the nitrogen fixation was decreased.

CH_3OH was used as a sacrificial electron donor in photocatalysis; furthermore, the proton from CH_3OH reacted with N_2 easier than that from H_2O in this study. As presented in Fig. 2b, there was no trace of NH_3 detected during nitrogen fixation over CNK1 in the dark. The ammonia evolution rate was decreased by half when the 100% CH_3OH reaction solution was substituted by 20% CH_3OH as well as 80% H_2O. Previous studies have found that the surface energy of a g-C_3N_4 layer is about 115 mJ m^{-2}, the surface energy of water is 102 mJ m^{-2}, and the surface energy of methanol is 71.38 mJ m^{-2}. The surface energy of H_2O is similar to that of the CN catalysts, which leads to weak adsorption between H_2O and CN. Since the surface energy of methanol is much lower than that of CN, methanol can be agglomerated on the surface of CN, and it is easier for the proton in methanol to take part in nitrogen

reduction. On the one hand, CH_3OH reacted with the holes on the photocatalyst to increase the photogenerated electrons. On the other hand, CH_3OH was easily adsorbed on the surface of the catalyst to take part in the subsequent reduction reaction as a proton donor and part of the electron donor. Moreover, the photocatalytic activity of CNK1 can be well retained even after keeping the product in the reaction solution for several cycles, as shown in the inset of Fig. 2b.

The efficiency of the photocatalytic nitrogen fixation is determined by the synergistic effects of the three basic steps of photocatalysis: (i) light absorption, (ii) carrier separation and transfer, and (iii) nitrogen dissociation and reduction. At rst, the optical properties of the as-synthesized samples were investigated through UV-vis absorption spectra (Fig. S4†). There was no change in the absorption edges (475 nm) of the CNKs as compared to those of CN. The absorption of light provided enough energy for the photocatalysts, and CNK1 achieved a high apparent quantum yield of 21.5% at 420 nm mono-chromatic light. The photoluminescence (PL) emission originating from the radiative recombination of the electron–hole pair was used to reveal the migration, transfer, and separation of photogenerated charge carriers. PL spectra of the CNKs are presented in Fig. 3a. The shift in the peak position was consistent with the variation in the KOH concentration. The CNK sample upon treatment with KOH at high concentrations had a smaller PL emission wavelength. The results indicated the faster carrier separation and transfer by K doping, as evidenced by the XPS and XRD results. Pristine CN had a strong PL emission peak as compared to CNKs. The broken structure of CNK increased the number of structural defects, which could capture the electrons or holes, thus resulting in a lower PL emission. Time-resolved photoluminescence decay spectra were also determined, and the results are shown in Fig. 3b. The change in the tendency of the decay time could be clearly identified. The treatment of CNK with KOH led to the decrease of the fluorescence lifetime in comparison with the case of the pristine CN sample. The fluorescence decays of the as-prepared samples are consistent with the decrease of PL intensities. Based on the results, the decrease in the PL intensity and decay time was attributed to the appropriate band structure, which promoted the separation of photogenerated carriers.

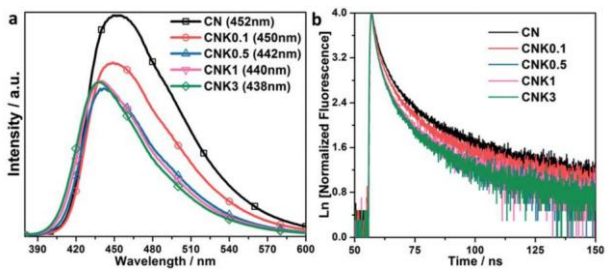

Fig. 3 Photoluminescence characterizations of the g-C_3N_4 and CNK samples. (a) PL spectra of the as-prepared catalysts and (b) time-resolved photoluminescence decay spectra of the as-prepared carbon nitrides. The spectra were obtained with the excitation of 340 nm from a picosecond pulsed light-emitting diode at room temperature.

To further confirm the transfer efficiency of charge carriers in the samples, transient photocurrent was also determined by electrochemistry. As presented in Fig. 4a, the samples showed a continuous increase following the incremental doping content of K due to the promoting charge separation and transfer. CH_3OH played an important role in the reduction process. Fig. 4b reveals the photocurrents of different amounts of CH_3OH added into the Na_2SO_4–H_2O electrolyte over CNK1 samples. The photocurrent increased 4 times and 6 times by introducing only 0.4% and 1.8% CH_3OH into the Na_2SO_4–H_2O electrolyte, respectively, as compared to that of the pure Na_2SO_4–H_2O electrolyte. However, when the content of CH_3OH was up to 3.8%, the photocurrent declined. The reason of the enhancement was that CH_3OH could react with the photo-generated holes in the catalysts. CH_3OH as a hole scavenger and electron donor increased the carrier transfer as well as the photocurrent. On the other hand, the proton from CH_3OH also participated in the reaction of nitrogen fixation, a reduction process requiring six electrons, which would capture electrons and decrease the photocurrent, directly showing the reactivity of nitrogen fixation. These two reactions complemented each other and gradually reached the equilibrium state, as shown by

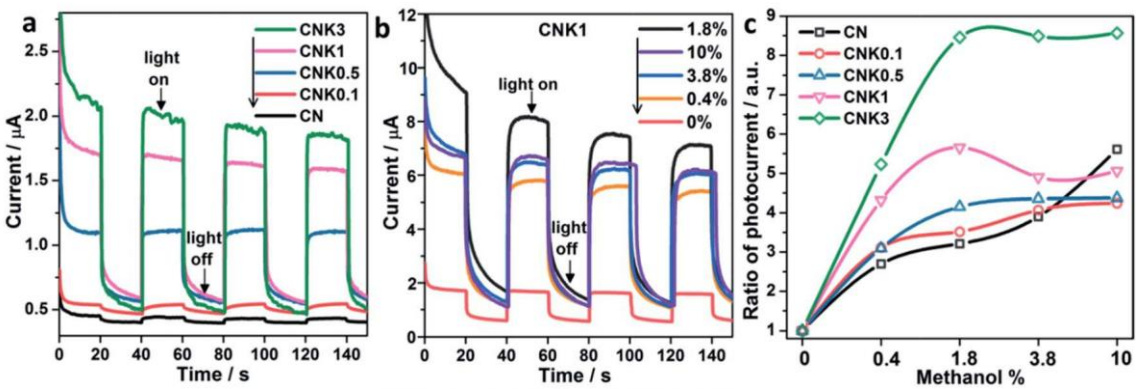

Fig. 4 Transient current curves over the g-C_3N_4 and CNK samples. (a) Comparison of different samples in the Na_2SO_4–H_2O electrolyte, (b) comparison of different CH_3OH addition amounts in the Na_2SO_4 water electrolyte for CNK1 samples, and (c) CH_3OH addition amount – transient current curves over CN and CNKs.

the photocurrent. The summary of the photocurrent under different addition amounts of CH_3OH over CN and CNKs is shown in Fig. 4c. The reactivity of CN with nitrogen was weak; thus, the photocurrent of 10% CH_3OH became larger than that for the other amounts. CNKs showed better nitrogen fixation performance; similarly, the photocurrent tended to stabilise when the CH_3OH amount increased. In particular, CNK1 presented a small decrease at 3.8% CH_3OH, suggesting the well reactivity with CH_3OH.

As aforementioned, nitrogen activation was the critical step in nitrogen fixation. The temperature-programmed desorption (TPD) investigations were used to understand N_2 activation on the surface of CN and CNK1. In Fig. 5, the peaks at 360 C of CN and 400 C of CNK were ascribed to chemical adsorption, and the intensity of the CN peak was much weaker than that of the CNK peak. Even for physical adsorption, the peak at 90 C of CN was slightly weaker than the peak at 120 C of CNK1. The desorption temperature of N_2-TPD on CNK1 was 30 C higher than that of CN. The larger intensity and desorption temperature of N_2-TPD on CNK confirmed the outstanding nitrogen activation by the broken structure.

It is worth mentioning that after the photocatalytic reaction on CNK1, the sample changed from pristine yellow to ash green. However, the ash green sample changed back to yellow after placing it in air for about one hour (Fig. S5†). To better under-stand the ammonia evolution process, isotope labelling in the solid C_3N_4 was measured at the Shanghai Engineering Research Center of Stable Isotope. The Thermo Scientific MAT 271 mass spectrometer was used in a dynamic mode, and a molecular ow sample gas inlet allowed accurate prediction of mass discrimination at the point of effusion of the gas after the burning of C_3N_4 at high temperatures in the mass spectrometer source. After the nitrogen fixation process on CNK1 under a $^{15}N_2$ atmosphere, the CNK1 sample was calcined at 400 C for one hour to remove the adsorbed nitrogen. Then, the ^{15}N content of the CNK1 sample was measured to be 0.39 atom%. This indicated that nitrogen in the C_3N_4 structure was reacted

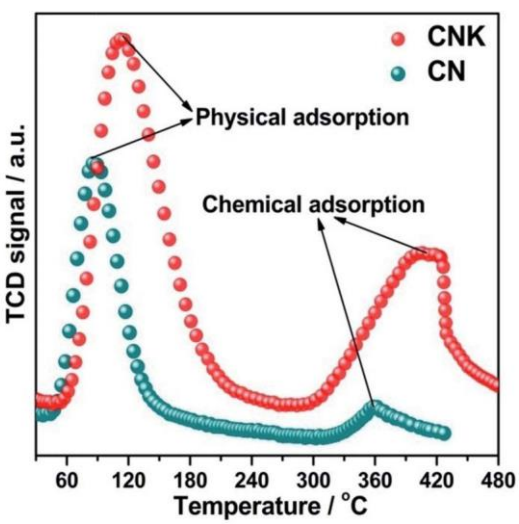

Fig. 5 N_2-TPD of CN and CNK1.

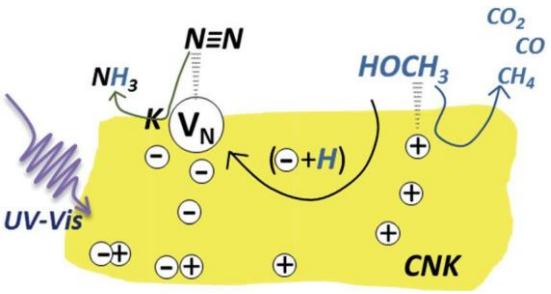

Scheme 1 The proposed mechanism of the photocatalytic N_2 fixation model in which CH_3OH serves as both the solvent and proton source.

with the proton in CH_3OH, and the produced vacancies could adsorb and activate N_2. The adsorbed N_2 was dissociated and reacted with the CH_3OH continuously. For catalytic nitrogen reduction to ammonia, nitrides are more beneficial since nitrogen atoms are already incorporated into their structure. This means that nitrogen atoms in the first surface layer of nitrides can in principle be reduced directly to ammonia and leave an N-vacancy on the surface. This N-vacancy then needs to be replenished by adsorption of a N_2 molecule to endure the catalytic cycle. This is known as the MvK mechanism, and the reaction of CN with CH_3OH under light irradiation follows this mechanism. The MvK mechanism existing in the CN–CH_3OH system stemmed from the N structure in CN and the reactivity of CH_3OH with CN catalysts. This was the reason why C_3N_4 had a ^{15}N atom in the structure and the color changed. CNK1 had little ammonia evolution (Fig. 2b) under an Ar atmosphere without N_2; this was not only a result of the chemically adsorbed N_2 on the surface, but also because nitrogen in the C_3N_4 structure reacted with CH_3OH under light irradiation.

The products, including CO_2, CO, and CH_4, of CH_3OH in the photocatalysis process were investigated. In other photo-catalysis processes, the products of CH_3OH oxidation are usually H_2, CO_2, or HCHO;[32,33] however, in this study, H_2 and HCHO are not detectable or are present in a negligible amount. The CH_3OH oxidation process was complicated, and further explorations were required. With these results in hand, although the precise mechanism was ambiguous, the general mechanism (Scheme 1) of CNK in the case would be as follows: nitrogen was adsorbed on the surface vacancies, and the photogenerated electrons and methanol-hole-generated protons transferred to nitrogen; this resulted in the formation of ammonia.

Conclusions

Methanol was first used as a proton source in photocatalytic Nitrogen fixation with the g-C_3N_4 catalyst. The etching of catalysts by KOH introduced the breakage of C]N in s-triazine of g-C_3N_4 and the graft of K ion. With an increase in the KOH concentration, the charge separation and ammonia evolution were promoted. However, an overlarge KOH concentration will lead to the destructive breakage and even decrease of exposed active sites for the adsorption of reaction species. The well

ammonia evolution rate 3.632 mmol g ^{1} h ^{1} of CNK1 resulted in synthetic effects, including the absorption of light energy, the enhanced solubility of N_2 in methanol, the adsorption of nitrogen on the exposed active sites, the generation of proton from CH_3OH, the promoted carrier transfer aroused by K and CH_3OH, and ammonia desorption bene ted from K on the surface. Overall, the use of CNK and CH_3OH suggests that CNK may work as an efficient nitrogen activation catalyst and represent a paradigm for a cost-efficient yet powerful photo-catalytic nitrogen fixation system only with sunlight as the energy source. The MvK catalytic mechanism was speculated in the CN–CH_3OH systems. Similar studies are also expected to be evoked for other photocatalyst materials with a nitrogen activation structure.

Experimental

Preparation of the catalysts

In a typical synthesis procedure, 10 g of urea was placed in a semi-closed alumina crucible with a cover. The crucible was heated to 550 C at a heating rate of 10 C min ^{1} in a tube furnace and maintained at this temperature for 3 h. A er thermal treatment, the crucible was cooled down to room temperature in the tube furnace. Then, pristine g-C_3N_4 was obtained a er washing and drying and labeled as CN. A er this, 0.2 g of CN was dissolved in 6 mL of KOH solution (0.1 M, 0.5 M, 1 M, and 3 M) and stirred for 3 h. The obtained solution was then washed by deionized water and ethanol several times until pH 7 and then dried at 80 C overnight to obtain the solid precursors. The resulting samples were obtained for further use and marked as CNK0.1, CNK0.5, CNK1, and CNK3.

Characterization of the photocatalysts

The purity and crystallinity of the as-prepared catalyst samples were characterized by powder X-ray diffraction (XRD) via a Rigaku D/MAX 2250 V diffractometer using monochromatized Cu Ka (l ¼ 0.15418 nm) radiation, and the voltage and electric current were held at 40 kV and 100 mA, respectively, over the range of 5 # 2q # 60 . The morphology and microstructure characterizations were performed using a transmission electron microscope (TEM, JEOL JEM-2100F, accelerating voltage 200 kV). UV-vis diffuse reflectance spectra (DRS) of the samples were obtained using a UV-vis spectrophotometer (Hitachi U-3010). X-ray photoelectron spectroscopy (XPS) was performed using an ESCALAB 250, Thermo Scientific Ltd. with a 320 mm diameter spot of monochromated aluminum Ka X-rays at 1486.6 eV under ultrahigh-vacuum conditions. The C 1s signal was used to correct the charge effects. Raman spectra were obtained using the Renishaw InVia system with a laser operating at l ¼ 785 nm as an excitation source. Fourier transform infrared (FTIR) spectra measurements were carried out using the FTS-3000 Fourier transform infrared spectrophotometer with KBr as the reference sample. Nitrogen temperature-programmed desorption (N_2-TPD) measurements were per-formed using the ChemiSorb 2750 instrument. Typically, 100 mg of the sample, placed in a glass tube, was pretreated with a He gas ow at 150 C for 2 h and then cooled down to 50 C. The adsorption of N_2 was performed in a 99.999% N_2 gas ow for 2 h at 50 C. After He gas purging, the sample was heated from 50 C to 450 C at a rate of 10 C min ^{1}. The TPD signal was obtained by a thermal conductivity detector. All the gas ow rates were set as 25 mL min ^{1}. Room temperature photoluminescence (PL) was conducted using the Hitachi F-4600 fluorescence spectrophotometer.

Photocatalytic tests

Photocatalytic tests were performed under the irradiation of a Xe lamp at room temperature (25 C). In each test without special statement, 20 mg of catalyst powder was used for each catalyst sample and put into 150 mL CH_3OH (99.7%, Sinopham chemical reagent Co. Ltd., China) solution. After 60 min, they were irradiated with a 300 W Xe light source through an Air Mass 1.5 G filter (ca. 100 mW cm ^{2}), and NH_4^+ was measured by a spectrophotometer with the Nessler's reagent through the dilution of methanol reaction solution with deionized water over 100 times.

The apparent quantum efficiency (AQY) for hydrogen production was measured using the wavelength of 420 nm band-pass filters. The AQY was calculated by the following equation:

$$\text{AQY (\%)} = \frac{\text{number of evolved } NH_3 \text{ molecules} \times 6}{\text{number of incident photons}} \times 100$$

NH_3/NH_4^+ concentration analysis

NH_3/NH_4^+ concentration analysis was conducted using the Nessler's reagent method.[34] At first, 150 mL of the suspension was filtered through a 0.22 mm membrane filter and then placed in a 50 mL sample tube after 100 times dilution. Then, 1 mL of the potassium sodium tartrate solution was added to the sample tube. After blending, 1 mL of Nessler's reagent was added to the same sample tube and mixed. Then, the mixture was le to stand for 10 min for full color processing. Finally, the concentration of NH_3/NH_4^+ was tested using a UV-vis spectro-photometer (Shimadzu UV-2550) at 420 nm wavelength.

Electrochemical analysis

The electrochemical analysis was performed via a CHI 660D electrochemical workstation (Shanghai Chenhua, China) using a standard three-electrode quartz cell. A Xe lamp (CHF-XM500) was used as a light source. To make a working electrode, catalyst powders were deposited on a fluorine-doped tin oxide (FTO) substrate by Na on coating. Brie y, 5 mg of catalyst was sus-pended in 3 mL of ethanol solution, and the mixtures were ultrasonically scattered for 30 min. Then, 200 mL of the above-mentioned slurry was coated on the FTO glass. After evaporation of ethanol, the catalyst-coated FTO substrate was used as the working electrode. During the photocurrent measurements, the current–time curves were obtained at 0.2 V vs. SCE, and the electrolyte was a 0.1 M Na_2SO_4 solution (pH 6.8) that was bubbled with nitrogen.

Conflicts of interest

There are no conflicts of interest to declare.

Acknowledgements

We acknowledge the financial support received from the National Basic Research Program of China (51772312, 21671197, 51472260) and the research grant obtained from the Shanghai Science and Technology Commission (16ZR1440800).

Notes and references

1 B. Askevold, J. T. Nieto, S. Tussupbayev, M. Diefenbach, E. Herdtweck, M. C. Holthausen and S. Schneider, Nat. Chem., 2011, 3, 532.
2 O. Einsle, F. A. Tezcan, S. L. A. Andrade, B. Schmid, M. Yoshida, J. B. Howard and D. C. Rees, Science, 2002, 297, 1696.
3 J. W. Erisman, M. A. Sutton, J. Galloway, Z. Klimont and W. Winiwarter, Nat. Geosci., 2008, 1, 636.
4 I. Ra qul, C. Weber, B. Lehmann and A. Voss, Energy, 2005, 30, 2487.
5 G. N. Schrauzer and T. D. Guth, J. Am. Chem. Soc., 1977, 99, 7189.
6 N. Cherkasov, A. O. Ibhadon and P. Fitzpatrick, Chem. Eng. Process., 2015, 90, 24.
7 K. Honkala, A. Hellman, I. N. Remediakis, A. Logadottir, A. Carlsson, S. Dahl, C. H. Christensen and J. K. Norskov, Science, 2005, 307, 555.
8 H. Li, J. Shang, Z. Ai and L. Zhang, J. Am. Chem. Soc., 2015, 137, 6393.
9 X. M. Li, W. Z. Wang, D. Jiang, S. M. Sun, L. Zhang and X. Sun, Chem.–Eur. J., 2016, 22, 13819.
10 G. Dong, W. Ho and C. Wang, J. Mater. Chem. A, 2015, 3, 23435.
11 S. Sun, Q. An, W. Wang, L. Zhang, J. Liu and W. A. Goddard Iii, J. Mater. Chem. A, 2017, 5, 201.
12 Y. Lu, Y. Yang, T. Zhang, Z. Ge, H. Chang, P. Xiao, Y. Xie, L. Hua, Q. Li, H. Li, B. Ma, N. Guan, Y. Ma and Y. Chen, ACS Nano, 2016, 10, 10507.
13 S. Sun, X. Li, W. Wang, L. Zhang and X. Sun, Appl. Catal., B, 2017, 200, 323.
14 K. Hoshino, R. Kuchii and T. Ogawa, Appl. Catal., B, 2008, 79, 81.
15 J. Liu, T. Zhang, Z. Wang, G. Dawson and W. Chen, J. Mater. Chem., 2011, 21, 14398.
16 S. Li, X. Chen, S. Hu, Q. Li, J. Bai and F. Wang, RSC Adv., 2016, 6, 45931.
17 H. Wei, Q. Zhang, Y. Zhang, Z. Yang and D. Dionysiou, Appl. Catal., A, 2016, 521, 9.
18 Z. Sun, J. Fischer, Q. Li, J. Hu and L. Wang, Appl. Catal., B, 2017, 216, 146.
19 G. Li, L. Li, H. Yuan, H. Wang and J. Shi, J. Colloid Interface Sci., 2017, 495, 19.
20 P. Iyngaran, D. C. Madden, D. A. King and S. J. Jenkins, J. Phys. Chem. C, 2014, 118, 12184.
21 T. Xiong, W. Cen, Y. Zhang and F. Dong, ACS Catal., 2016, 6, 2462.
22 H. Zhang, L. Zhao, F. Geng, L.-H. Guo, B. Wan and Y. Yang, Appl. Catal., B, 2016, 180, 656.
23 J. Xu, L. Zhang, R. Shi and Y. Zhu, J. Phys. Chem. A, 2013, 1, 14766.
24 K. H. Park, B. H. Kim, S. H. Song, J. Kwon, B. S. Kong, K. Kang and S. Jeon, Nano Lett., 2012, 12, 2871.
25 F. Dong, Y. Li, Z. Wang and W. Ho, Appl. Surf. Sci., 2015, 358, 393.
26 H. X. Wu, D. Y. Chen, N. J. Li, Q. F. Xu, H. Li, J. H. He and J. M. Lu, Nanoscale, 2016, 8, 12066.
27 M. Groenewolt and M. Antonietti, Adv. Mater., 2005, 17, 1789.
28 Z. Zhou, J. Wang, J. Yu, Y. Shen, Y. Li, A. Liu, S. Liu and Y. Zhang, J. Am. Chem. Soc., 2015, 137, 2179.
29 V. O. Njoku, K. Y. Foo, M. Asif and B. H. Hameed, Chem. Eng. J., 2014, 250, 198.
30 Y. Shiraishi, S. Kanazawa, Y. Sugano, D. Tsukamoto, H. Sakamoto, S. Ichikawa and T. Hirai, ACS Catal., 2014, 4, 774.
31 P. V. Zinin, L.-C. Ming, S. K. Sharma, V. N. Khabashesku, X. Liu, S. Hong, S. Endo and T. Acosta, Chem. Phys. Lett., 2009, 472, 69.
32 M. Bowker, D. James, P. Stone, R. Bennett, N. Perkins, L. Millard, J. Greaves and A. Dickinson, J. Catal., 2003, 217, 427.
33 T. Kawai and T. Sakata, J. Chem. Soc., Chem. Commun., 1980, 694.
34 R. H. Leonard, Clin. Chem., 1963, 9, 417.